Available online at www.sciencedirect.com

ScienceDirect

Procedia Engineering 147 (2016) 13 – 19

Procedia Engineering

www.elsevier.com/locate/procedia

11th conference of the International Sports Engineering Association, ISEA 2016

A comparison of the wake structures of scale and full-scale pedalling cycling models

T. N. Crouch[a,*], D. Burton[a], J. A. Venning[a], M. C. Thompson[a], N. A. T. Brown[b], and J. Sheridan[a]

[a]*Department of Mechanical and Aerospace Engineering, Monash University, Clayton, VIC 3800, Australia*
[b]*Australian Institute of Sport, Belconnen, ACT 2617, Australia*

Abstract

This paper presents a novel approach to better understand the unsteady aerodynamics associated with a dynamically pedalling cyclist. Using high resolution Particle Image Velocimetry (PIV) in a water channel, the large-scale wake structure is analysed for various phases of the crank cycle of a 1:4.5 scale-model cyclist/bicycle under both static and pedalling conditions. Both quasi-steady and dynamic pedalling leg results are compared with detailed velocity field surveys made in the wake of a full-scale pedalling cyclist mannequin of similar geometry and position in a wind tunnel. A time-averaged and phase-averaged analysis of the various flow regimes that occur throughout the pedal stroke shows good agreement between scale-model and full-scale mannequin investigations. This highlights the robustness of the formation of the primary wake flow structures when subjected to varying Reynolds number, bicycle/rider geometry and quasi-steady/dynamic pedalling conditions.

Peer-review under responsibility of the organizing committee of ISEA 2016

Keywords: Aerodynamics; bluff-body; sports; cycling; wake structure; vortex flows.

1. Introduction

Optimising aerodynamics is one of the most effective ways to gain a significant competitive advantage and performance gains in elite cycling. This is why leading nations and teams allocate significant resources to improving the aerodynamics of their athletes. Central to elite level cycling performance is the role that aerodynamic drag has on the speed and power requirements of cyclists. The aerodynamic drag component has been shown to account for up to 90% of the total resistive forces acting on cyclists travelling on relatively flat surfaces for speeds > 8.9 m/s [1]. This coupled with the fact that the power required to overcome aerodynamic drag 'P_{Aero}' varies with the freestream velocity cubed means that the overwhelming majority of the power output by cyclists at racing speeds goes into overcoming aerodynamic resistance [2].

Cyclists competing in individual cycling events have two options for reducing aerodynamic drag. Riders can minimise their projected frontal area 'A' and/or reduce their drag coefficient 'C_D'. Rider position has been shown to

* Corresponding author. Tel.: +61-399-059-253.
E-mail address: timothy.crouch@monash.edu

Peer-review under responsibility of the organizing committee of ISEA 2016
doi:10.1016/j.proeng.2016.06.182

have the largest influence on these variables, followed by equipment selection and design [1,3,4]. As the frontal area and drag coefficient is influenced simultaneously when optimising position and equipment, predicting aerodynamic drag is often difficult due to the highly non-linear relationship between A and C_D. Through a better understanding of the three dimensional flows around cyclists and the primary fluid mechanisms having the largest influence on drag, informed decisions and potentially new optimal methods for reducing drag can be sought.

Recent advances in our understanding of flows around cyclists have come from improved experimental and numerical techniques. With advances in computer-aided-design (CAD) and manufacturing methods such as 3D-printing and CNC-machining, high resolution and detailed models can be produced from scanned data and 3D computer modelling. These numerical models of the rider/bicycle geometry can then in-turn be used as an input into computational fluid dynamic simulations (CFD). Numerical studies by Griffith *et al.* [5,6] and Defraeye *et al.* [7,8] have shown that such methods provide an effective additional tool for optimising and investigating cycling aerodynamics when run in parallel with an experimental program.

Experimental and numerical studies by Crouch *et al.* [9] and Griffith *et al.* [5] have shed light onto the dominant fluid mechanisms influence cycling aerodynamics by characterising the large-scale flow structures that develop in the wake. Wind tunnel investigations of Crouch *et al.* mapped the time-averaged flow in the wake of a full-scale mannequin for various static leg positions around a full 360° revolution of the crank. Large changes in the flow structure and aerodynamic drag, which varied up to 20%, was measured around the crank cycle. The major flow structure variants were characterised into symmetrical and asymmetrical flow regimes and were associated with low and high drag states. A low drag symmetrical flow regime corresponded to crank angles near to horizontal that resulted in the alignment of the upper thighs of both legs. The high drag asymmetrical state was found for crank angles where one leg was in a raised and the other in an extended position. For these phases of the crank cycle, a strong streamwise counter-rotating vortex pair that originates from the hip region of the mannequin was the primary wake feature. These findings were compared with investigations of the flow around a numerical model of the mannequin by Griffith *et al.* who found a good match in the downstream wake structure.

More recently investigations by Crouch *et al.* [10] have extended the quasi-steady understanding of the wake by investigating the large-scale wake structure under dynamic pedalling leg conditions. Phase-averaged velocity field measurements with a full-scale mannequin showed (for realistic racing cadences) the primary symmetric and asymmetric wake features were consistent for both the quasi-steady and dynamic leg results. This investigation continues to build upon our understanding of the three dimensional flow around the complete bicycle-rider system for dynamic leg conditions. This is achieved using a novel technique which incorporates a moving leg scale-model produced using 3D printing methods for highly resolved velocity field measurements obtained using PIV in a water channel.

2. Experimental Method

Figure 1 (a) shows the full-scale wind tunnel mannequin and the 1:4.5 scale water channel model. The models are both depicted in the 15° leg position which is defined as the crank angle 'θ'. The zero degree leg position corresponds to when the cranks are horizontally aligned with the left leg in a downstream location. The plastic scale-model rider and bicycle frame was manufactured using a Stratasys Object Connex 500 3D printer. The highest print resolution setting was used (print layers of 30μm) and a conservative estimate puts the printing tolerance at 0.2 mm. Although minor design changes have been made to the scale-model, the major geometric features and dimensions have been scaled directly from the full-scale CAD wind tunnel mannequin geometry, detailed in Crouch *et al.* [9]. Alterations to the scale-model geometry have been made to allow for the rotation of the legs, 'smooth' surface transitions between intersecting limbs and ease of replacing body-parts. Features such as the head and helmet have been scaled directly from high resolution scanned data.

The major difference between the 1:4.5 scale and full-scale model is the bicycle frame and wheel geometry. The bike frame used in the wind tunnel studies is now outdated and was first released over 10 years ago. The simplified scale-model bicycle is based on the geometry of current Time-Trial (TT) bicycles from leading manufacturers. The major dimensions and cross-section characteristics of the frame members non-dimensionalised by the wheel base WB (229 mm) are detailed in table 1. In addition to the bicycle frame the wheels have been modelled as flat disks instead of open spoke wheels.

(a) Wind tunnel (top) and water channel (bottom) models.

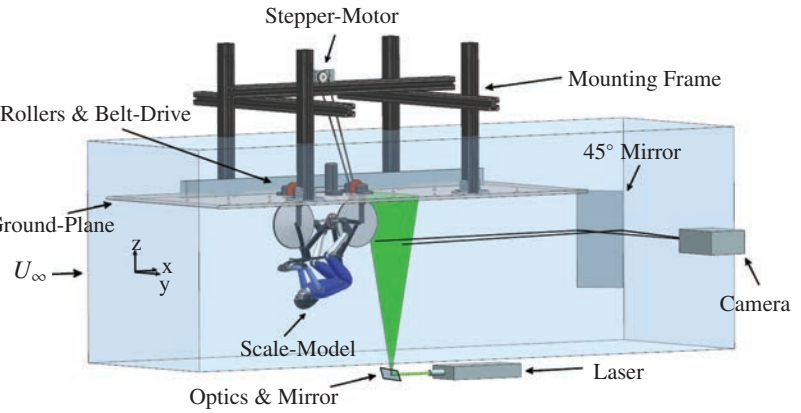

(b) Water channel 1:4.5 scale-model.

Fig. 1. (a) Full-scale (top) and 1:4.5 scale (bottom) cycling models. (b) Experimental set-up of the scale model in the water tunnel.

PIV wake measurements with the scale-model were undertaken in the $0.6 \times 0.8 \times 4.0m$ working section of the Fluids Laboratory for Aeronautical and Industrial Research (FLAIR) free-surface water channel. The freestream test speed was 0.4 m/s which corresponds to a Reynolds number Re of 5.7×10^4 based on the torso chord length c. (Note: Re of full-scale wind tunnel tests compared in this study was 6.9×10^5). At this freestream velocity the test section turbulence intensity I_u is $< 1\%$ and the flow uniformity is within $\pm 1\%$ [11].

Figure 1 (b) depicts the scale-model set-up in the water channel. The model was rigidly mounted upside down to a ground plane via struts attached either side of the front and rear wheel axles. The ground plane extended 2WB upstream and 2.5WB downstream of the leading and trailing edges of the model respectively. The struts were of a symmetrical airfoil profile section and positioned the rubber front and rear wheel tires on the friction drive mechanism.

Table 1. Scale-model TT-bicycle dimensions (non-dimensionalised with respect to the wheel base length).

Member	Length	Cross-section	Defining Dimension	Angle
AB	0.507	NACA 0035	$chord = 0.052$	$\beta = 80°$
BC	0.552	11:8 Ellipse	$major_{radius} = 0.02$	$\gamma = 3°$
CD	0.090	NACA 0035	$chord = 0.134$	$\tau = 69°$
AD	0.641	NACA 0035	$chord = 0.078$	-
DE	0.430	NACA 0035	$chord = 0.050$	$\tau = 69°$
AF	0.376	2:5 Rectangle	$width = 0.021$	$\mu = 70°$
BF	0.516	NACA 0035	$chord = 0.041$	-
$Crank$	0.164	-	$x_{hip} = 0.188$, $y_{hip} = 0.803$	-
$Wheels$	-	Disk	$\phi = 0.673$, $width = 0.022$	-
$Torso\ (c)$	0.646	Comp-Ellipse	-	$\alpha = 15°$

The drive consisted of an electric micro-stepper-motor (50,800 steps/rev) located above the water surface which powered rollers underneath each wheel connected via a 1:1 timing belt drive system. As the wheels were made to rotate, the legs would be driven around the crank cycle through the 1:4.44 fixed gear chain and sprocket bicycle drivetrain. For all dynamic tests the legs were made to rotate at a cycling frequency f of 0.19 Hz (11.5 RPM). At

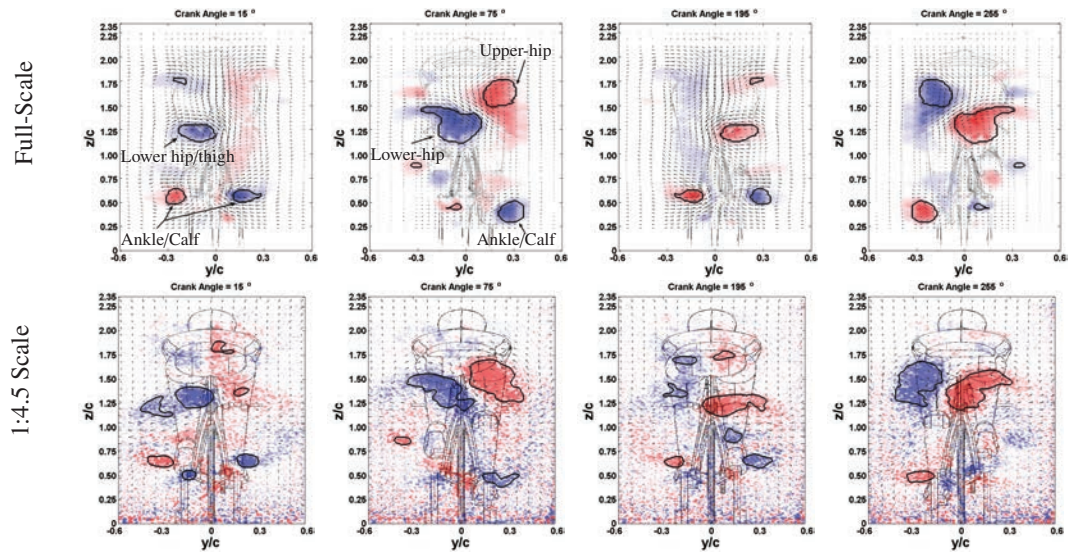

Fig. 2. Contours of the time-averaged streamwise vorticity fields obtained a torso length behind the hips with in-plane velocity vectors overlaid for static full-scale and 1:4.5 scale-model leg positions (quasi-steady results). The top and bottom rows show the full-scale and scale vorticity fields respectively with respect to the spatial coordinates non-dimensionalised by the torso chord length c. Contours vary from blue to red across the range $-100s^{-1} <= \omega_x <= 100s^{-1}$. Solid lines show vortices identified using the swirling strength criterion.

this cycling cadence and gearing the wheel ground speed matched the water channel freestream velocity. This also corresponds to a reduced pedalling frequency 'k', defined as the ratio of the leg speed around the crank to the forwards riding velocity, of 0.11 which matched the conditions of the full-scale wind tunnel tests performed at elite level racing speeds and cadences (16 m/s at 100 RPM).

PIV vector fields were obtained in a plane normal to the freestream flow a torso length $x/c = 1$ downstream of the model rider. The flow was seeded using Vestosint spherical particles (Vestosint, Germany) with a mean size and density of 20 μm and 1.106 g/cm^3 respectively. The particles were illuminated by a light sheet generated from two Minilite II Continuum lasers (New Wave Research Inc., USA) in combination with a series of optical components. Using a mirror positioned at 45° to the mean flow downstream of the model a pco.4000 CCD camera, with a 105 mm lens, was used to record image pairs of the spanwise plane. The resulting 2160×4008 (effective area) image pairs were analysed using in-house software by Fouras *et al.* [12] with a window size of 32 by 32 pixels and an overlap of 75%. With each pixel representing an area of $85.6 \times 85.6\mu m$ this resulted in a 267×498 vector field, evenly spaced at 0.7 mm intervals.

Velocity fields were measured for both static and dynamic leg positions and are directly compared with similar full-scale wind tunnel results. For the dynamic tests, phase averaged velocity fields were determined for a number of leg positions around the crank cycle from PIV data binned into ±10° regions about these crank angles. Phase-averaged velocity fields are the result of 222 image pairs recorded in each bin. The uncertainty of the velocity vectors associated with the variability of binned data was 2% U_∞ for a 95% confidence level. So that static and dynamic results can be directly compared, dynamic leg positions used to label phased-averaged results have been corrected for the lag in crank angle that results from the time it takes the flow to convect downstream to the measurement plane. This was achieved assuming a convection velocity of $0.6U_\infty$ as outlined in Crouch *et al.* [9]. For further details on this correction and details of the experimental method used to obtain phase averaged wake data with the full-scale wind tunnel mannequin please refer to this study.

3. Results And Discussion

Compared in figure 2 are contours of the time-averaged (static-legs) streamwise vorticity fields for the scale-model and full-scale mannequin at the low and high drag leg positions. Despite differences in the geometry of the two

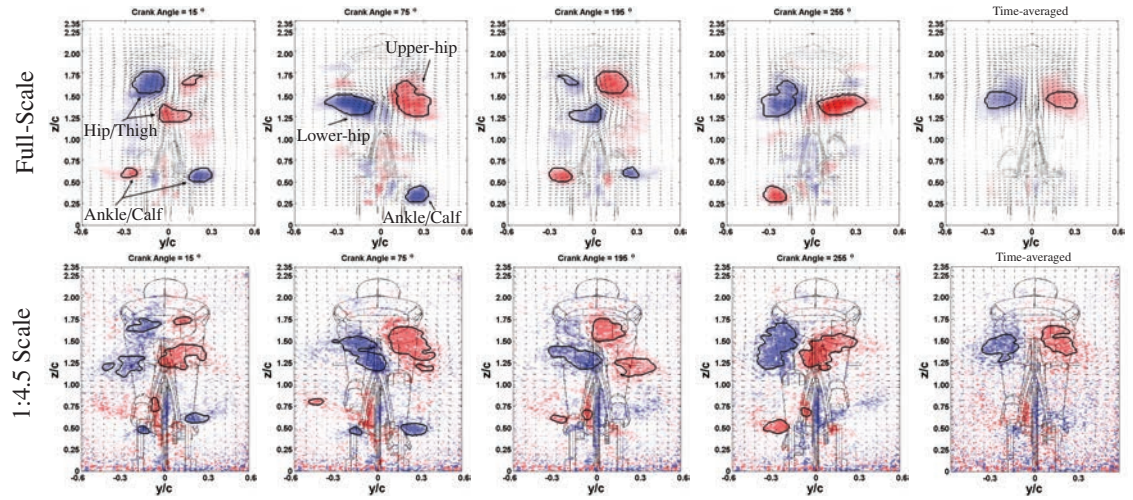

Fig. 3. Contours of the phase-averaged and time-averaged streamwise vorticity fields obtained a torso length behind the hips with in-plane velocity vectors overlaid for dynamic full-scale and 1:4.5 scale-model leg positions (results for $k = 0.11$). The top and bottom rows show the full-scale and scale vorticity fields respectively with respect to the spatial coordinates non-dimensionalised by the torso chord length c. Contours vary from blue to red across the range $-100s^{-1} <= \omega_x <= 100s^{-1}$. Solid lines show vortices identified using the swirling strength criterion.

rider/bicycle models and an order of magnitude separating the *Re* at which water channel and wind tunnel tests were performed, there is good agreement between both sets of results. For the 15° leg position when the upper legs are aligned the in-plane velocity vectors and the streamwise vorticity contours show a relatively symmetrical flow field when compared with the high drag 75° asymmetrical leg position. This is especially true for areas of the wake $> 1.5y/c$ where the flow shows very good symmetry about the centre plane. In the second half of the crank cycle these findings are also reflected. Opposite leg positions 180° out of phase (15° and 195°, 75° and 255°) show very good symmetry about the centre plane. (Note: Symmetry is enforced across the centre plane for opposite leg positions 180° out of phase for the full-scale wind tunnel results, see Crouch *et al.* [10] for details.)

To highlight the major flow structures of each flow regime, streamwise vortices have been identified using the swirling strength criterion of Zhou *et al.* [13]. Although the level of detail of the wake structure of the 1:4.5 scale-model is higher than the full-scale mannequin, as a result of the higher spatial resolution of the PIV flow fields, similar streamwise vortices are outlined using this vortex identification scheme in figure 2 for both sets of results. The dominant and most consistent wake feature is the upper and lower hip-vortices that form a large streamwise counter rotating vortex pair for the 75° and 255° asymmetrical leg positions. A smaller well defined vortex is also observed in the wake of the ankle/calf of the straightened leg. These large-scale and well defined flow structures compare very well between the water channel and wind tunnel studies and show good consistency in their location, size, irregular shape and strength. For the symmetrical 15° and 195° positions a reasonable comparison is also made between both data sets. At these crank angles the large scale hip-vortices are either no longer identified or are significantly reduced in size and strength. Coherent streamwise vortices of opposite sign, identified in the wake of both left and right ankles/calves, also compare well between water channel and wind tunnel results.

Figure 3 shows phase-averaged contours of the streamwise vorticity fields for the scale and full-scale models pedalling at a reduced frequency of 0.11. As with the the quasi-steady results the phase-averaged findings, depicted for the high and low drag leg positions, are in good agreement with both data sets. The large-scale flow structures labelled using the swirling strength criterion, for the asymmetrical 75° and 255° crank angles compare very well. Once again the location, size, irregular shape and strength of the hip-vortex pair as well as the smaller ankle/calf vortex are in excellent agreement between scale and full-scale flows. These large-scale flow structures also match up well with there quasi-steady counterparts from the static leg flow fields. The good agreement between static and dynamic results shows that for analysing the wake structure a quasi-steady assumption is reasonable for leg positions of the asymmetrical flow regime. For a regular cycling cadence the legs and flow is predominantly in an asymmetrical state and therefore this constitutes the majority of the crank cycle.

The persistence of the large-scale asymmetric hip-vortices in a time-average sense is indicated in figure 3 by the time-averaged vorticity field for pedalling leg conditions. The streamwise vortices that originate behind the hips are clearly evident in the time-averaged dynamic leg wake. For the water channel flow field, derived from PIV measurements sampled at 12 Hz (non-harmonic of the pedalling frequency), the symmetry in the flow field across the centre plane reflects the good flow symmetry that was observed for opposite leg positions. The similarity in the time-averaged wake structure between the scale and full-scale flow fields also reflects the good agreement in phase-averaged results between the two data sets that was observed for leg positions other than those hilighted in figures 2 and 3.

As with the quasi-steady findings the phased-averaged flow field for the symmetrical 15° and 195° leg positions are in reasonable agreement between the scale and full-scale tests. Minor differences in both data sets can be found in the lower wake regions. Unlike the high drag asymmetrical leg positions the dynamic and static leg flow fields for the symmetrical flow regime do not compare as well. Remnants of the large-scale flow structures from the preceding asymmetrical flow regime are evident in both the 15° and 195° leg position phase-averaged flow fields. As a result of this the same degree of symmetry in this flow regime is not achieved when comparing with the static leg results. This may partially result from the bin size used to obtain the phase averaged flow fields, although these findings are also reflected in the full scale results which used a much smaller bin size in the phase averaging process (6° compared to 20°). This suggests a lag in the transition from asymmetric to symmetric flow regimes than what otherwise would not be observed under quasi-steady conditions. Despite these differences a reduction in the size and strength of the large-scale wake structures is found and is consistent with what one would expect from the low drag flow regime.

4. Conclusion

In this experimental investigation a novel technique for investigating the wake structure of a cyclist, using a 1:4.5 scale-model in a water channel, was tested and compared with full-scale data. High resolution PIV flow fields of the scale-model were compared with similar measurements performed in a wind tunnel using a full-scale mannequin pedalling at realistic elite level cadences and riding speeds. Despite the significant offset in *Re* and variations in the geometry of the models (body/bicycle), good agreement between the flow fields of both models was observed for both quasi-steady and pedalling conditions. This was shown for both symmetric and asymmetric flow regimes and highlights the robustness of the formation of the primary wake structures. A comparison of quasi-steady and phase-averaged flow fields showed a closer match for asymmetrical leg positions and that a quasi-steady approximation is a reasonable approach to investigating the cyclist wake up to the reduced pedalling frequencies tested.

References

[1] Kyle, C.R. and Burke, E.R., Improving the racing bicycle, *Mechanical Engineering*, **106(9)**, 1984, 34–45.
[2] Hosoi, A.E., Drag kings: characterizing large-scale flows in cycling aerodynamics, *Journal of Fluid Mechanics*, **748**, 2014, 1–4.
[3] Jeukendrup, A.E., and Martin, J., Improving cycling performance: how should we spend our time and money, *Sports Medicine*, **31(7)**, 2001, 559–569.
[4] Zdravkovich, M., Achcroft, M., Chrisholm, S., and Hicks, N., Effect of cyclists posture and vicinity of another cyclist on aerpdynamic drag, *The Engineering of Sport*, **1**, 1996, 21–28.
[5] Griffith, M.D., Crouch, T.N., Thompson, M.C., Burton, D., Sheridan, J. and Brown, N.A.T., Computational Fluid Dynamics Study of the Effect of Leg Position on Cyclist Aerodynamic Drag, *Journal of Fluids Engineering*, **136(10)**, 2014, 101105.
[6] Griffith, M.D., Crouch, T.N., Thompson, M.C., Burton, D., and Sheridan, J., Elite Cycling Aerodynamics: Wind Tunnel Experiments and CFD, Proceedings of the 18th Australasian Fluid Mechanics Conference, Tasmania, Australia, 2012.
[7] Defraeye, T., Blocken, B., Koninckx, E., Hespel, P. and Carmeliet, J., Computational fluid dynamics analysis of cyclist aerodynamics: Performance of different turbulence-modelling and boundary-layer modelling approaches, *Journal of biomechanics*, **43(12)**, 2010, 2281–2287.
[8] Defraeye, T., Blocken, B., Koninckx, E., Hespel, P. and Carmeliet, J., Aerodynamic study of different cyclist positions: CFD analysis and full-scale wind-tunnel tests, *Journal of biomechanics*, **43(7)**, 2010, 1262–1268.
[9] Crouch, T.N., Burton, D., Brown, N.A.T., Thompson, M.C., and Sheridan, J., Flow topology in the wake of a cyclist and its effect on aerodynamic drag, *Journal of Fluid Mechanics*, **748**, 2014, 5–35.
[10] Crouch, T.N., Burton, D., Thompson, M.C., Martin, D.T., Brown, N.A.T., and Sheridan, J., A Phase-Averaged Analysis of the Pedalling Cyclist Wake, Proceedings of the 19th Australasian Fluid Mechanics Conference, Melbourne, Victoria, Australia, 2014.
[11] Venning, J., Jacono, D.L., Burton, D., Thompson, M. and Sheridan, J., The effect of aspect ratio on the wake of the Ahmed body, *Experiments in Fluids*, **56(6)**, 2015, 1-11.

[12] Fouras, A., Lo Jacono, D., and Hourigan, K., Target-free Stereo PIV: a novel technique with inherent error estimation and improved accuracy, *Experiments in Fluids*, **44(2)**, 2007, 317–329.

[13] Zhou, J., Adrian, R., Balachandar, S., and Kendall, T., Mechanisms for generating coherent packets of hairpin vortices in channel flow, *Journal of Fluid Mechanics*, **387**, 1999, 353–396.